Journal of Power Sources 238 (2013) 11–16

Contents lists available at SciVerse ScienceDirect

Journal of Power Sources

journal homepage: www.elsevier.com/locate/jpowsour

Evaluation of a brownmillerite oxide as cathode for solid oxide fuel cells

Qiang Li [a], Liping Sun [a], Xu Zeng [a], Hui Zhao [a,*], Lihua Huo [a], Jean-Claude Grenier [b], Jean-Marc Bassat [b], Fabrice Mauvy [b]

[a] Key Laboratory of Functional Inorganic Material Chemistry (Heilongjiang University), Ministry of Education, PR China
[b] ICMC Bordeaux-CNRS, 87 Avenue du Dr. A. Schweitzer, Université de Bordeaux 1, F-33608 Pessac-Cedex, France

HIGHLIGHTS

- $Ca_2Fe_{1.3}Mn_{0.7}O_{5+\delta}$ cathode material is studied for applications in SOFCs.
- Cathode material gave the lowest polarization resistance of 0.22 $\Omega\,cm^2$ at 750 °C.
- The rate limiting step for ORR depends on the oxygen partial pressure.

ARTICLE INFO

Article history:
Received 11 December 2012
Received in revised form
27 February 2013
Accepted 1 March 2013
Available online 14 March 2013

Keywords:
Solid oxide fuel cells
Brownmillerite oxide
Cathode material
Electrode reaction

ABSTRACT

Brownmillerite oxide $Ca_2Fe_{1.3}Mn_{0.7}O_{5+\delta}$ is synthesized and evaluated as a new cathode material for solid oxide fuel cells (SOFCs). The average thermal expansion coefficient (TEC) of $Ca_2Fe_{1.3}Mn_{0.7}O_{5+\delta}$ is $13.3 \pm 0.2 \times 10^{-6}\,K^{-1}$, close to that of the typical electrolyte materials. The lowest polarization resistance (R_p) ($0.22 \pm 0.02\,\Omega\,cm^2$ at 750 °C in air) and cathodic overpotential values are achieved when the material is sintered at 1000 °C on $Ce_{0.9}Gd_{0.1}O_{1.95}$ (CGO) electrolyte. Two main oxygen reduction reaction (ORR) processes are identified. The rate limiting step for ORR is found to depend on the oxygen partial pressure. The excellent electrochemical performance indicates that $Ca_2Fe_{1.3}Mn_{0.7}O_{5+\delta}$ can be a promising cathode material for SOFCs.

1. Introduction

Mixed ionic and electronic conducting oxides (MIEC) have promising applications in high-temperature electrochemical devices, such as ceramic membranes for oxygen separation, sensors and electrodes of solid oxide fuel cells (SOFCs) [1]. Many perovskite-type MIEC materials, such as $La_{1-x}Sr_xMnO_3$, $Ba_{0.5}Sr_{0.5}Co_xFe_{1-x}O_3$, La_2NiO_4 and $La_{2-x}Sr_xCuO_4$ have been extensively studied as possible cathodes in SOFCs [2–5].

Concerning the crystal structure, brownmillerite oxides (with the nominal formulation $A_2B_2O_5$) can be considered as oxygen-deficient perovskites where the oxygen vacancies ordered along (010) planes, forming one-dimensional diffusion pathway for oxygen ion migration in the tetrahedral layer [6,7]. Goodenough reported that the orthorhombic brownmillerite oxide $Ba_2In_2O_5$ exhibited high oxygen ionic conductivity at high temperatures [8]. Kharton studied the electrical property of $Ca_2AlFeO_{5+\delta}$ oxide. The results showed that $CaAlFeO_{5+\delta}$ had almost unit oxide ion transference number in air [9]. Recent studies proved the potential applications of some brownmillerite oxides in the separation of oxygen from air and partial oxidation of light hydrocarbons, which indicates that the brownmillerite compounds may exhibit relatively high ionic-electronic mixed conductivity and promising oxygen permeability [10,11]. Meanwhile in another study, the TEC of $Ca_2Fe_2O_5$ ceramic was found to be in the range of 11.3–$13.6 \times 10^{-6}\,K^{-1}$ [12], compatible with many solid electrolyte materials such as $Ce_{0.9}Gd_{0.1}O_{1.95}$ (CGO), $Sm_{0.2}Ce_{0.8}O_{1.95}$ (SDC) et al. These results encourage us to study the cathode properties of some brownmillerite oxides that derived from $Ca_2Fe_2O_5$ by doping with other cations [13,14]. It was found that both $Ca_2Fe_{2-x}Co_xO_{5+\delta}$ and $Ca_{2-x}Sr_xFe_2O_{5+\delta}$ show good electrochemical properties and catalytic activity, and the compound $Ca_2Fe_{1.8}Co_{0.2}O_{5+\delta}$ resulted in the lowest polarization resistance of 0.23 $\Omega\,cm^2$ at 700 °C in air.

Studies indicate that Mn^{4+} doping can strongly affect the Fe^{3+} oxidation state and the simultaneous formation of oxygen defects

* Corresponding author.
E-mail address: zhaohui98@yahoo.com (H. Zhao).

0378-7753/$ – see front matter © 2013 Elsevier B.V. All rights reserved.
http://dx.doi.org/10.1016/j.jpowsour.2013.03.010

in $Ca_2Fe_2O_5$, which are responsible for the catalytic activity and the electrical properties [15]. In another paper, Ramezanipour investigated $Ca_2Fe_{2-x}Mn_xO_{5+\delta}$ with respect to ordering of oxygen vacancy on both local and long-range length scales and their effect on crystal structure [16]. For the set with $\delta = 0$, the oxygen vacancies always order in the long-range sense to form the brownmillerite structure containing alternative layers of octahedrally and tetrahedrally coordinated cations. Akiyama reported [17] the electrical and magnetic properties of nonstoichiometric $Ca_2Fe_{2-x}Mn_xO_{5+\delta}$ and found that incorporating manganese ions into the iron sublattice changed the level of oxygen defects, and the electrical conductivity and magnetic properties improved. It was generally believed that these oxygen defects offered the possibility of rapid oxygen transport through the ceramic material.

In this work, the electrochemical properties of $Ca_2Fe_{1.3}Mn_{0.7}O_{5+\delta}$ material supported on $Ce_{0.9}Gd_{0.1}O_{1.95}$ (CGO) electrolyte and the kinetics of oxygen reduction reaction (ORR) of the electrode are studied.

2. Experimental

$Ce_{0.9}Gd_{0.1}O_{1.95}$ (CGO) powders were prepared according to Ref. [18]. The obtained powders were first pressed uniaxially at 220 MPa, and then sintered at 1400 °C for 10 h to form a pellet. The dense electrolyte ceramics were about 1 mm in thickness and 15 mm in diameter. $Ca_2Fe_{1.3}Mn_{0.7}O_{5+\delta}$ powders were synthesized using the solid-state reaction [19]. These powders were mixed with terpineol to form ink, which was subsequently painted on one side of the CGO electrolyte pellet to form working electrode (WE) with a surface area of 0.5 cm^2. Platinum paste was painted on the other side of the pellet in symmetric configuration, as the counter electrode (CE). A Pt wire was used as a reference electrode (RE) and put on the same side of the working electrode. Pt gauze attached to a Pt wire was used as the current collector. The cell was first heated at 400 °C to eliminate organic binders, followed by sintering at 1000 °C for 4 h in air.

The structure and phase purity of the prepared powders were investigated by an X-ray powder diffraction on a Rigaku D/MAX-3B diffractometer using the Cu-K_α radiation. The morphology and microstructure of the sintered electrodes were examined by Hitachi S-4700 FEG-SEM (field emission gun-scanning electron microscope). The conductivity of $Ca_2Fe_{1.3}Mn_{0.7}O_{5+\delta}$ was measured with the d.c. four terminal method using Keithley 2400 digital source meter and AI 808P program temperature controller controlled by computer, from room temperature to 800 °C in air. Thermal expansion behavior was measured with Setsys Evolution TMA system (SETARAM, France). The measurements were carried out in air with a heating rate of 5 °C min^{-1} from room temperature to 800 °C. The impedance spectra were recorded over the frequency range 1 MHz to 0.1 Hz using Autolab PGStat30 potentiostat, with the imposed AC voltage 10 mV. The measurements were performed at equilibrium potential (OCV) as a function of temperature (500–750 °C) and oxygen partial pressure (in an N_2/O_2 mixed atmosphere). The electrochemical impedance spectra (EIS) fitting were performed with the Zview software. The dc polarization experiments were performed by the chronoamperometry method [20], which involved a potential step followed by recording the current density as a function of time. The cathode overpotential was calculated according to the following relation:

$$\eta_{WE} = \Delta U_{WR} - iR_{el}$$

where represents the cathode overpotential, ΔU_{WR} is the applied voltage between working electrode and reference electrode, i is the current flowing through the test cell and R_{el} is the resistance of the electrolyte obtained from the impedance spectrum.

3. Results and discussions

3.1. Chemical stability of the cathode material

Fig. 1a shows the XRD pattern and the refinement profile for $Ca_2Fe_{1.3}Mn_{0.7}O_{5+\delta}$ powders. As expected, $Ca_2Fe_{1.3}Mn_{0.7}O_{5+\delta}$ crystallize in a single phase with space group *Pnma* (62), no impurities are found. The calculated lattice parameters are $a = 5.3717(3)$ Å, $b = 14.9039(7)$ Å, $c = 5.4799(3)$ Å and $V = 438.72(4)$ $Å^3$. These values are quite similar to the reported $Ca_2Fe_{2-x}Mn_xO_{5+\delta}$ [15–17]. The result is consistent that $Ca_2Fe_{1.3}Mn_{0.7}O_{5+\delta}$ belongs to brownmillerite-type material. It is known that in some cases, the interfacial chemical reaction between the cathode and the electrolyte is undesirable for long term stability of SOFCs, which may increase the interfacial polarization resistance and thus resulting in degradation of the performance [21]. The possible chemical reaction between $Ca_2Fe_{1.3}Mn_{0.7}O_{5+\delta}$ cathode and CGO electrolyte was further investigated. In general, $Ca_2Fe_{1.3}Mn_{0.7}O_{5+\delta}$ was mixed thoroughly with CGO powders in 1:1 weight ratio to form a mixture, and then sintered at 1100 °C for 24 h in air. The obtained powders were checked by XRD. The corresponding diffraction patterns were refined and the results are presented in Fig. 1b.

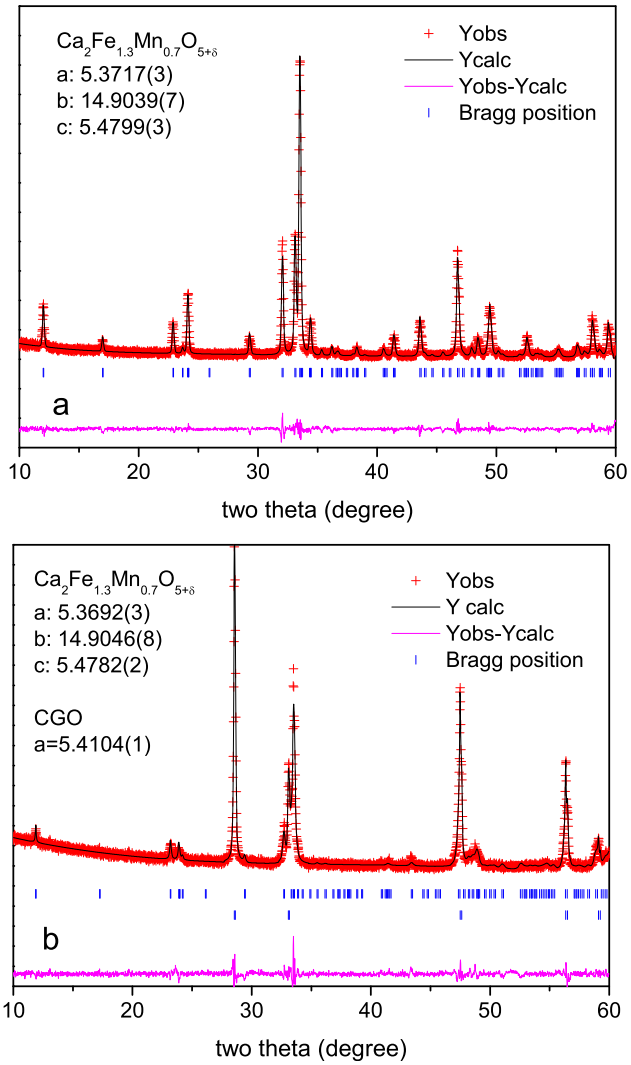

Fig. 1. XRD patterns and the refinement profiles for (a) $Ca_2Fe_{1.3}Mn_{0.7}O_{5+\delta}$ and (b) $Ca_2Fe_{1.3}Mn_{0.7}O_{5+\delta}$–CGO mixtures after sintered at 1100 °C for 24 h in air.

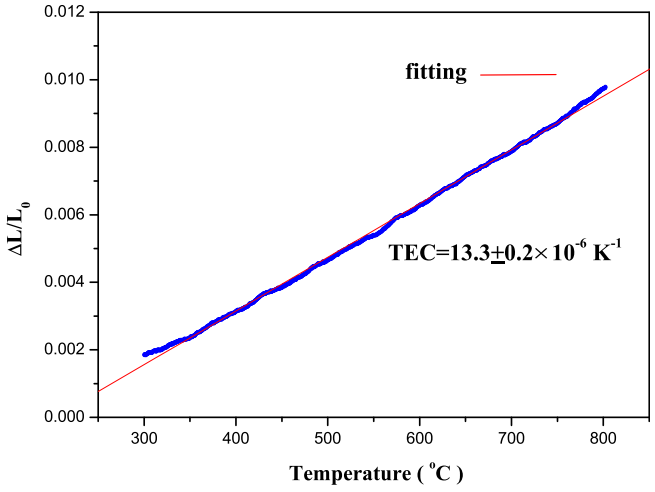

Fig. 2. Thermal expansion curve for $Ca_2Fe_{1.3}Mn_{0.7}O_{5+\delta}$ material.

Clearly, all these diffraction peaks can be refined well with $Ca_2Fe_{1.3}Mn_{0.7}O_{5+\delta}$ and CGO. There are no new peaks identified or shift of XRD peaks observed in the patterns. The lattice parameters of the two components in the mixture remain unchanged after the heat-treatment. This result indicated no reaction and/or inter-diffusion of elements occurred between $Ca_2Fe_{1.3}Mn_{0.7}O_{5+\delta}$ and CGO at temperatures up to 1100 °C.

The mismatch of the TEC between the cathode and electrolyte always results in delamination of the cathode/electrolyte interface, or cracking of the electrolyte because of the stress development upon heating and cooling cycle [22]. Therefore the TEC value of the prepared $Ca_2Fe_{1.3}Mn_{0.7}O_{5+\delta}$ was measured. Fig. 2 shows the thermal expansion curve of the $Ca_2Fe_{1.3}Mn_{0.7}O_{5+\delta}$ sample over a temperature range of 300–800 °C in air. The average TEC of $Ca_2Fe_{1.3}Mn_{0.7}O_{5+\delta}$ is $13.3 \pm 0.2 \times 10^{-6}$ K^{-1} in 300–800 °C, which is much closer to that of CGO electrolyte (TEC, is 13.5×10^{-6} K^{-1}) [23]. This implies that $Ca_2Fe_{1.3}Mn_{0.7}O_{5+\delta}$ might be more suitable as a cathode based on CGO electrolyte for intermediate temperature solid oxide fuel cells (IT-SOFCs).

3.2. Electrochemical measurements of the cathode material

Arrhenius plot of the electrical conductivity of $Ca_2Fe_{1.3}Mn_{0.7}O_{5+\delta}$ is presented in Fig. 3. The conductivity, σ, was measured in the temperature range of 300–800 °C in air. The activation energy for conduction was calculated from the linear region in the plot, using the following expression derived for the small polaron mechanism [24]:

$$\sigma = \frac{A}{T}\exp\left(\frac{-E_a}{kT}\right)$$

where A is the preexponential factor, k is the Boltzmann constant, T is the absolute temperature and E_a is the activation energy. The electrical conductivity of $Ca_2Fe_{1.3}Mn_{0.7}O_{5+\delta}$ increased gradually with temperature, indicating the conducting behavior of semiconductors. The σ value reached to 6.5 S cm^{-1} at 800 °C in air, which is much higher than that of the un-doped $Ca_2Fe_2O_5$ material (0.6 S cm^{-1}, at 800 °C) [12]. On the other hand, an inflexion point was observed around 450 °C in the Arrhenius plot, with two different slopes obtained in the temperature range 300–450 °C and 450–800 °C. The calculated activation energies were 0.58 eV and 0.42 eV, respectively. In a previous study of nonstoichiometric $Ca_2Fe_{2-x}Mn_xO_{5+\delta}$ ($x = 0.3, 0.5$) [17], the change of activation energy with temperature was observed at about 450 °C. This phenomenon was ascribed to the oxygen order-disorder phase transition at high temperature. Considering their quite similar composition and crystal structure, we propose the same reason for the change of activation energy with temperature that observed in the material $Ca_2Fe_{1.3}Mn_{0.7}O_{5+\delta}$.

Fig. 4 shows a typical impedance spectrum of the $Ca_2Fe_{1.3}Mn_{0.7}O_{5+\delta}$ cathode that sintered at 900 °C for 4 h on the CGO electrolyte and then measured at 650–750 °C in air. In the impedance spectrum, two arcs were observed to locate in the high-frequency and low-frequency zone, respectively. This indicates that the oxygen reduction reaction (ORR) over the electrode is composed of at least two different processes. In order to clarify this point, an equivalent circuit was used to fit the measuring data (Fig. 4, inset). Here R_{el} represents the intercept value of the impedance spectrum at high frequency side with the real axis, which corresponds to the resistance of the electrolyte and lead wires. R_H and R_L are the resistance corresponding to the high frequency and low frequency arcs, respectively. The electrode polarization resistance (R_p) is the sum of R_H and R_L. CPE is constant phase element whose value reflects the reaction mechanism of different electrode processes. As expected, an increase of the measurement temperature resulted in a significant reduction of the polarization resistance (R_p). The R_p value of $Ca_2Fe_{1.3}Mn_{0.7}O_{5+\delta}$ at 750 °C was 0.22 ± 0.02 Ω cm^2 in air, lower than

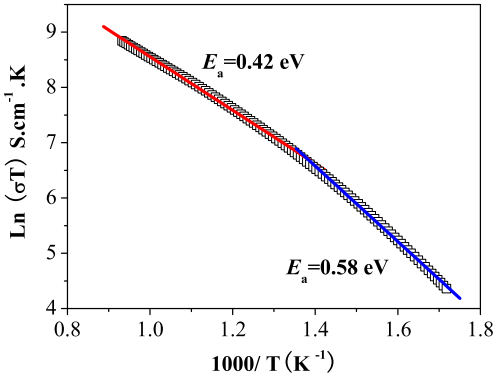

Fig. 3. Arrhenius plot of electrical conductivity for $Ca_2Fe_{1.3}Mn_{0.7}O_{5+\delta}$.

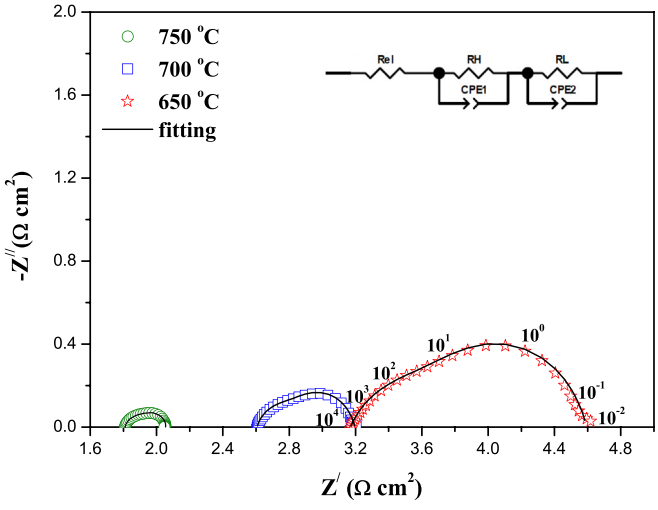

Fig. 4. Impedance spectra for $Ca_2Fe_{1.3}Mn_{0.7}O_{5+\delta}$ cathode measured at 650–750 °C in air.

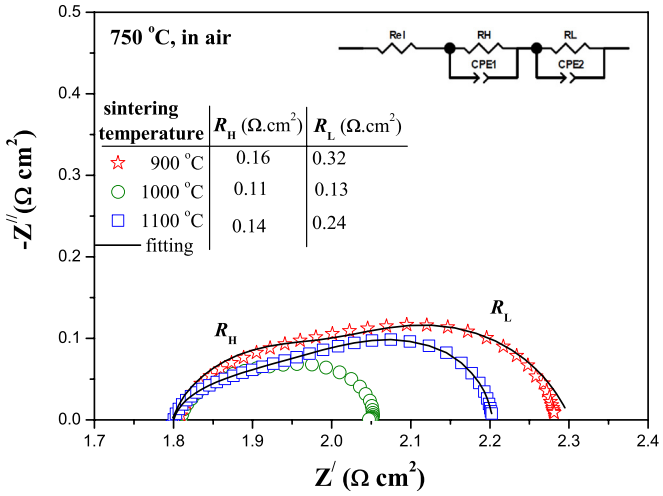

Fig. 5. Impedance spectra for $Ca_2Fe_{1.3}Mn_{0.7}O_{5+\delta}$ cathode sintered at different temperatures for 4 h and then measured at 750 °C in air.

the reported $GdBaCo_2O_{5+\delta}$ and $SmBaCu_2O_{5+\delta}$ cathodes [25,26], but is still higher than those of well-known materials, such as $La_{0.6}Sr_{0.4}Co_{0.2}Fe_{0.8}O_3$ (LSCF) [27].

In order to investigate the effect of sintering temperature on the cathode performance, different sintering conditions were studied. Fig. 5 shows the impedance spectrum of the $Ca_2Fe_{1.3}Mn_{0.7}O_{5+\delta}$ cathode after sintered at different temperatures for 4 h and then measured at 750 °C in air. From the fitting results, it can be found that the low frequency arc dominant in spectra and the values of R_L are always larger than those of R_H. By calculation, it is found that both R_H and R_L show dependence on sintering temperature. R_L decreases about 59.37 %, at the same time R_H decreases 31.25 %, when the sintering temperature changes from 900 to 1000 °C. R_H and R_L increased again when the sintering temperature is up to 1100 °C.

It is well known that sintering temperature has considerable effect on the electrode microstructure, which in turn will influence the electrode performance. Therefore, the microstructure evolution of the $Ca_2Fe_{1.3}Mn_{0.7}O_{5+\delta}$ cathode was further studied as a function of sintering temperature. The SEM images of $Ca_2Fe_{1.3}Mn_{0.7}O_{5+\delta}$ cathode sintered at different temperatures are exhibited in Fig. 6. It can be seen that $Ca_2Fe_{1.3}Mn_{0.7}O_{5+\delta}$ particles form poor contact with each other when the sintering temperature was 900 °C (Fig. 6a). After sintered at 1000 °C, a fine microstructure with moderate porosity and well-necked particles was formed. The average particle size of $Ca_2Fe_{1.3}Mn_{0.7}O_{5+\delta}$ is about 2 μm (Fig. 6b). $Ca_2Fe_{1.3}Mn_{0.7}O_{5+\delta}$ combined quite well with the CGO to form good contact electrode/electrolyte interface, and the thickness of the cathode is about 30 μm (Fig. 6d). This porous microstructure is beneficial to the improvement of the cathode property, as that proved in Fig. 4. When the cathode was further sintered at 1100 °C for 4 h, however, particle agglomeration phenomenon was observed (Fig. 6c). This will retard the oxygen reduction reaction by decreasing the triple phase boundary (TPB) length, and at the same time blocking the oxygen gas diffusion into the bulk cathode. The similar over-sintering effect has been observed before in the other cathode materials [28]. Hereafter, the studied cathodes were finally sintered at 1000 °C for 4 h to obtain the best sintering performance.

To study the oxygen reduction reaction (ORR) mechanism occurring on the cathode, impedance spectrum of $Ca_2Fe_{1.3}Mn_{0.7}O_{5+\delta}$ cathode was measured as a function of oxygen partial pressure.

Fig. 7 presents the dependence of the cathode polarization resistances (R_p) on oxygen partial pressure (P_{O_2}). Generally, R_p varies with the oxygen partial pressure according to the following equation:

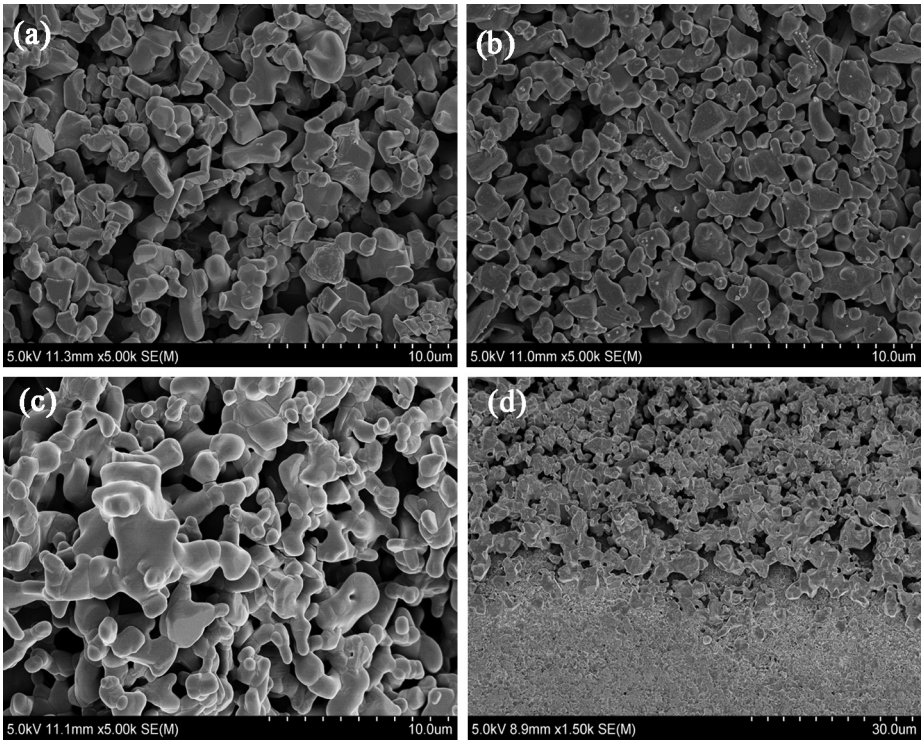

Fig. 6. SEM images of $Ca_2Fe_{1.3}Mn_{0.7}O_{5+\delta}$ electrode sintered at (a) 900 °C; (b) 1000 °C; (c) 1100 °C and (d) the cross-section image of the test cell.

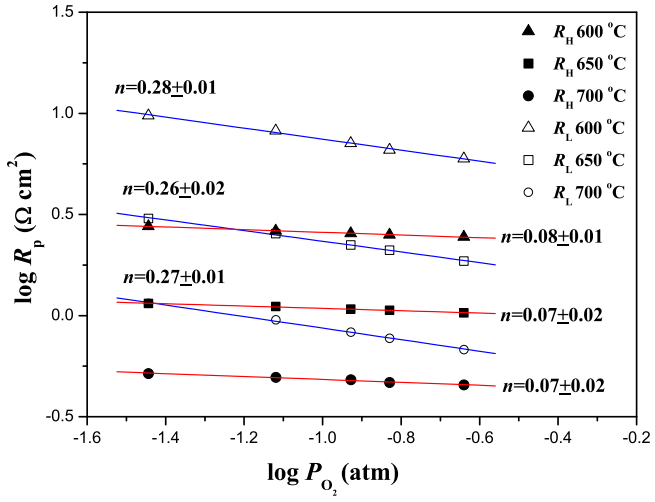

Fig. 7. Oxygen partial pressure dependence of polarization resistance for $Ca_2Fe_{1.3}Mn_{0.7}O_{5+\delta}$ cathode.

$$R_P = R_P^0 (P_{O_2})^{-n}$$

$n = 1/2$, $O_{2,ads} \rightleftarrows 2O_{ads.}$ (oxygen surface adsorption, dissociation and surface diffusion)
$n = 1/4$, $O_{ads.} + 2e' + V_O^{\cdot\cdot} \rightleftarrows O_O^x$ (charge transfer process)
$n = 0$, $O_{TPB}^{2-} + V_O^{\cdot\cdot} \rightleftarrows O_O^x$ (oxygen ion transfer into the electrolyte)

The value of n may give useful information about the type of species involved in the electrode reactions [29,30]. For metal oxide electrodes on solid electrolytes, $n = 0$ has been attributed to the oxygen ion transfer from the TPB to the electrolyte, $n = 0.25$ related to the charge transfer process on the electrode, occurring at the current collector/electrode and the electrode/electrolyte interfaces, respectively, and $n = 0.5$ to the oxygen adsorption-desorption process, involving oxygen diffusion at the gas/cathode surface interface and surface diffusion of intermediate oxygen species related.

As it can be seen, a 0.26–0.28 P_{O_2} dependency of R_L is observed at 600–700 °C. Therefore the low frequency arc can be assigned to the charge transfer process on the electrode. The characteristic of R_H showed quite weak P_{O_2} dependency (n value is 0.07–0.08), which could be related to the oxygen ion diffusion within the bulk electrode and/or from electrode to CGO electrolyte through tripe phase boundary (TPB). From the fitting results (Fig. 7), it is further observed that the resistance of the low frequency arc (R_L) is always larger than that of the high frequency arc (R_H) at low oxygen partial pressure. R_L is closer to R_H with the increase of oxygen partial pressure. Therefore, it is concluded that two different kinds of reaction rate limiting steps exist on the $Ca_2Fe_{1.3}Mn_{0.7}O_{5+\delta}$ cathode, depending on the oxygen partial pressure. At low oxygen partial pressure, the reaction rate limiting step is charge transfer process. With increasing the oxygen partial pressure from N_2 to air, the reaction rate limiting step would be a mixed process involving successively the charge transfer and oxygen ion diffusion within the bulk electrode. The complex cathode behavior observed for $Ca_2Fe_{1.3}Mn_{0.7}O_{5+\delta}$ material is partially due to the easy variation of oxygen stoichiometry of this compound.

The $\log i - \eta$ characteristic for $Ca_2Fe_{1.3}Mn_{0.7}O_{5+\delta}$ cathode at different temperatures is reported in Fig. 8. A Tafel behavior is observed; the exchange current density can be directly obtained from the extrapolated intercept of the Tafel plots at $\eta = 0$. The exchange current density increases with the temperature ($i_0 = 3.1$ mA cm^{-2} at 600 °C, $i_0 = 6.8$ mA cm^{-2} at 650 °C, $i_0 = 18.2$ mA–cm^{-2} at 700 °C). A comparison with literature data is difficult as various parameters may influence the electrode properties, for instance, the geometry of the cell, the deposition technique, and the shaping of the electrode. However, the $i - \eta$ characteristics of the $Ca_2Fe_{1.3}Mn_{0.7}O_{5+\delta}$ electrode show promising performance compared to the lanthanum manganites [31, 32].

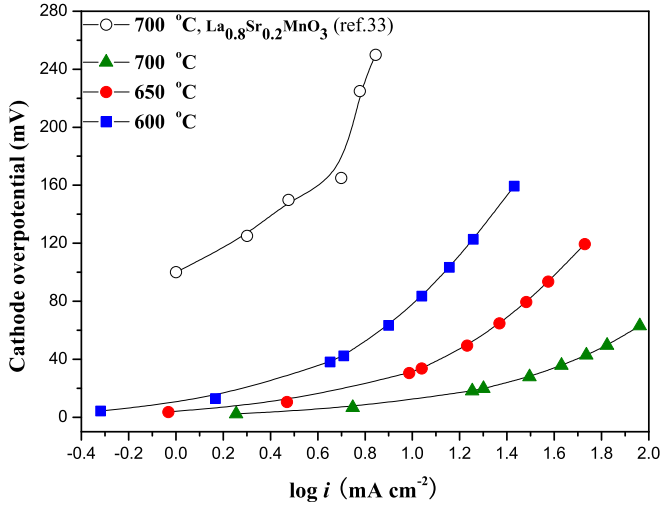

Fig. 8. Polarization curve for $Ca_2Fe_{1.3}Mn_{0.7}O_{5+\delta}$ cathode that measured at different temperatures in air.

4. Conclusions

In this work, a brownmillerite oxide $Ca_2Fe_{1.3}Mn_{0.7}O_{5+\delta}$ have been synthesized by solid state reaction and assessed for possible use in SOFCs. $Ca_2Fe_{1.3}Mn_{0.7}O_{5+\delta}$ cathode forms good contact with the CGO electrolyte after sintering at 1000 °C for 4 h. No chemical reaction was found between $Ca_2Fe_{1.3}Mn_{0.7}O_{5+\delta}$ electrode and the CGO electrolyte. The thermal expansion coefficient (TEC) of $Ca_2Fe_{1.3}Mn_{0.7}O_{5+\delta}$ is $13.3 \pm 0.2 \times 10^{-6}$ K^{-1} at 300–800 °C, which is closed to that of CGO electrolyte. The reaction rate limiting step for oxygen reduction on the electrode is the charge transfer process. The lowest polarization resistance obtained at 750 °C in air is about 0.22 ± 0.02 Ω cm^2. The polarization curve of $Ca_2Fe_{1.3}Mn_{0.7}O_{5+\delta}$ reveals promising behavior as an SOFC cathode.

Acknowledgements

This work was supported by National Natural Science Foundation of China (51072048, 51102083, 51110105016, 51210105009),

Program for Science and Technology Project of Heilongjiang Province (WB10A204), Natural Science foundation of Heilongjiang Province (JC201211, B201107).

References

[1] D. Brett, A.D. Brett, A. Atkinson, N.P. Brandon, S.J. Skinner, Chem. Soc. Rev. 37 (2008) 1568–1578.
[2] R.F. Tian, J. Fan, Y. Liu, C.R. Xia, J. Power Sources 185 (2008) 1247–1251.
[3] Z. Shao, S.M. Haile, Nature 431 (2004) 170–173.
[4] M. Escuderoa, A. Fuertea, L. Dazaa, J. Power Sources 196 (2011) 7245–7250.
[5] Q. Li, H. Zhao, L.H. Huo, L.P. Sun, X.L. Cheng, J.C. Grenier, Electrochem. Commun. 9 (2007) 1508–1512.
[6] P. Berastegui, S.G. Eriksson, S. Hull, Mater. Res. Bull. 34 (1999) 303–314.
[7] I.A. Leonidov, V.L. Kozhevnikov, M.V. Patrakeev, E.B. Mitberg, K.R. Poeppelmeier, Solid State Ionics 144 (2001) 361–369.
[8] J.B. Goodenough, J.E. Ruiz-Diaz, Y.S. Zhen, Solid State Ionics 44 (1990) 21–31.
[9] V.V. Kharton, I.P. Marozau, N.P. Vyshatko, A.L. Shaula, A.P. Viskup, E.N. Naumovich, F.M.B. Marques, Mater. Res. Bull 38 (2003) 773–782.
[10] J. Sunarso, S. Baumann, J.M. Serra, W.A. Meulenberg, S. Liu, Y.S. Lin, J.C. Diniz da Costa, J. Membr. Sci. 320 (2008) 13–41.
[11] W.S. Yang, H.H. Wang, X.F. Zhu, L.W. Lin, Top. Catal. 35 (2005) 155–167.
[12] A.L. Shaula, Y.V. Pivak, J.C. Waerenborgh, P. Gaczyñski, A.A. Yaremchenko, V.V. Kharton, Solid State Ionics 177 (2006) 2923–2930.
[13] Q. Li, L.P. Su, L.H. Huo, H. Zhao, J.C. Grenier, Int. J. Hydrogen Energy 35 (2010) 9151–9157.
[14] Q. Li, Z.H. Xue, H. Zhao, L.H. Huo, Chin. J. Inorg. Chem. 25 (2009) 1349–1353.
[15] T. Akiyama, Mat. Res. Bull. 16 (1981) 469–476.
[16] F. Ramezanipour, J.E. Greedan, L.M.D. Cranswick, V.O. Garlea, R.L. Donaberger, J. SiewenieCong, J. Am. Chem. Soc. 134 (2012) 3215–3227.
[17] T. Akiyama, Mat. Res. Bull. 16 (1981) 1077–1084.
[18] S.W. Zha, A. Moore, H. Abernathy, M.L. Liu, J. Electrochem. Soc. 151 (2004) A1128–A1133.
[19] A.P. Grosvenor, J.E. Greedan, J. Phys. Chem. C 113 (2009) 11366–11372.
[20] A. Espuirol, N. Brandon, N. Bonanos, J. Kilner, M. Mogensen, B.C.H. Steele, in: A.J. McEvoy (Ed.), Proceedings of the Fifth European Solid Oxide Fuel Cell Forum, U. Bossel, Oberrohrdorf, Switzerland (Publ.), 2002, pp. 225–232.
[21] A. Montenegro Hernández, L. Mogni, A. Caneiro, Int. J. Hydrogen Energy 35 (2010) 6031–6036.
[22] N.Q. Minh, T. Takahashi, Science and Technology of Ceramic Fuel Cell, Elsevier, Amsterdam, 1995. pp. 117–146.
[23] H. Hayashi, M. Kanoh, C.J. Quan, H. Inaba, S.R. Wang, M. Dokiya, H. Tagawa, Solid State Ionics 132 (2000) 27–233.
[24] J.A.M. Roosmalen, J.P.P. Huijsmans, L. Plom, Solid State Ionics 66 (1993) 279–284.
[25] J. Peña-Martínez, A. Tarancón, D. Marrero-López, J.C. Ruiz-Morales, P. Núñez, Fuel Cell 5 (2008) 351–359.
[26] X. Kong, X.F. Ding, Int. J. Hydrogen Energy 36 (2011) 15715–15721.
[27] M. Sahibzada, S.J. Benson, R.A. Rudkin, J.A. Kliilner, Solid State Ionics 113 (1998) 285–289.
[28] Q. Li, Y. Fan, H. Zhao, L.P. Sun, L.H. Huo, J. Power Sources 167 (2007) 64–68.
[29] R.A. Souza, J.A. Kilner, Solid State Ionics 106 (1998) 175–187.
[30] R.A. Souza, J.A. Kilner, Solid State Ionics 126 (1999) 153–161.
[31] M. Krumpelt, J. Ralph, T. Cruse, J.-M. Bae, in: J. Huismans (Ed.), The Fifth European Solid Oxide Fuel Cell Forum, 2002 pp. 215–224.
[32] J. Holc, D. Kuščer, M. Hrovat, S. Bernik, D. Kolar, Solid State Ionics 95 (1997) 259–268.